ACS chemical biology

Letters

pubs.acs.org/acschemicalbiology

Shuttling of PINK1 between Mitochondrial Microcompartments Resolved by Triple-Color Superresolution Microscopy

Felix R. M. Beinlich,[†] Christoph Drees, Jacob Piehler, and Karin B. Busch*[,‡]

Mitochondrial Dynamics Group and Biophysics Group, School of Biology, University of Osnabrück, 49076 Osnabrück, Lower Saxony, Germany

Supporting Information

ABSTRACT: The cytosolic *p*hosphatase and *ten*sin homologue Pten-kinase PINK1 involved in mitochondrial quality control undergoes a proteolytic process inside mitochondria. It has been suggested that the protein is not fully imported into mitochondria during this maturation. Here, we have established live cell triple-color superresolution microscopy by combining FPALM and tracking and localization microscopy (TALM) in order to unravel the spatiotemporal organization of the C-terminal kinase domain of PINK1 during this process. We find that the kinase domain is imported into active mitochondria and colocalizes with respiratory complex I at the inner mitochondrial membrane. When the processing step inside mitochondria is inhibited or mitochondria are de-energized, full length PINK1 distributes between the outer and the inner mitochondrial membranes, indicating a holdup of import. These findings give the molecular base for a dual role of PINK1—inside energized mitochondria and outside of de-energized mitochondria.

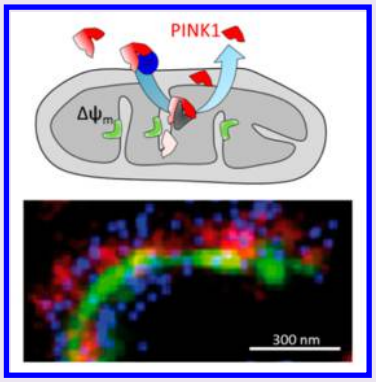

The cytosolic *p*hosphatase and *ten*sin homologue Pten-induced kinase 1 (PINK1) and Parkin1, a cytosolic E3 ubiquitin ligase, are key players in mitochondrial quality assurance.[1−4] Multifarious functions of PINK1 in mitochondrial quality control have been proposed[5,6] that remain controversially debated due to ambiguous information about the exact suborganellar localization of PINK1. PINK1 accumulates at the outside of (artificially) depolarized mitochondria, where it activates Parkin1 by phosphorylation at Ser65.[7] It was also reported that PINK1 protects against oxidative stress by phosphorylation of mitochondrial chaperone TNF receptor-associated protein 1 (TRAP1) inside mitochondria,[8] and that it regulates the mitochondrial protease Htr2a.[9] Furthermore, a relation between PINK1 and the phosphorylation status of respiratory complex I subunit NdufA10 was described.[10] These observations suggest that PINK1 is active at least in two different cellular compartments (cytosol and mitochondria), and possibly inside two mitochondrial subcompartments: in the intermembrane space and in the matrix. Full-length PINK1 (fl-PINK1, 63 kDa) is synthesized in the cytosol with a genuine mitochondrial targeting sequence (MTS) at the N-terminus. The PINK1 protein has a putative transmembrane sequence, a serine/threonine kinase domain, and a C-terminal regulatory domain (CTD, Figure 1a). Mutations in the kinase domain of PINK1 have been found in a number of Parkinson's patients.[11,12] Under normal conditions, PINK1 undergoes a maturation process inside mitochondria: After import of PINK1, the MTS is removed in the matrix.[13] The resulting fl-PINK1 protein is cleaved between the A103 and F104 (i.e., in the putative transmembrane domain, Figure 1a, arrowhead) by the presenilin-associated rhomboid-like (PARL) protease located in the inner mitochondrial membrane (IMM) to produce the matured 53 kDa short form (s-PINK1, ΔN-PINK1).[13−16] s-PINK1 is subsequently degraded by a proteasome inhibitor-sensitive process, which therefore very likely involves the export into the cytosol.[17] Usually, the turnover of PINK1 is high;[18] however, when F104 was mutated to A104, the short form s-PINK1 was predominant. In general, the processing and retranslocation of PINK1 is dependent on the mitochondrial membrane potential as the key feature of active mitochondria,[19] and in depolarized mitochondria, PINK1 remains at the outside of mitochondria in close proximity to the TOM complex.[20] Another mutation in the transmembrane domain at position 95 (P95A) shifted the ratio toward full length PINK1, albeit it did not abrogate the PINK1-PARL interaction.[16] The localization of the active kinase domain during PINK1 maturation and degradation is still equivocal.[19,21−23] One reason is that conventional biochemical analysis methods struggle with the constitutively low steady-state levels of PINK1 intermediates.

In order to resolve the intraorganellar trafficking of the PINK1 kinase domain during mitochondrial processing, we here introduce a novel approach for live cell triple-color superresolution (SR) imaging based on single molecule localization microscopy. For this purpose, we implemented dual-color tracking and localization microscopy (TALM) in combination with fluorescence photoactivation localization microscopy (F-PALM)[24,25] for probing the spatiotemporal organization of PINK1 in relation to marker proteins for mitochondrial

Received: April 26, 2015
Accepted: June 5, 2015
Published: June 5, 2015

DOI: 10.1021/acschembio.5b00295
ACS Chem. Biol. 2015, 10, 1970−1976

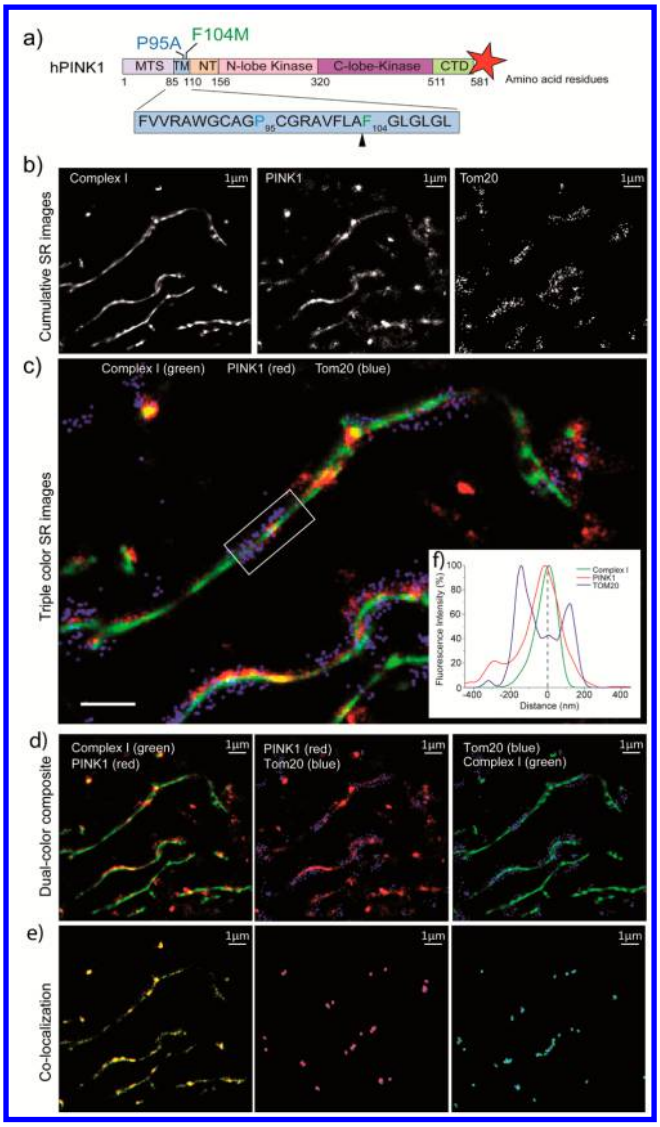

Figure 1. Live-cell super-resolution imaging of PINK1 in energized mitochondria in HeLa cells. (a) Scheme of PINK1 structure with the mutated residues P95 and F104 in the transmembrane domain (TM). The red star marks the tagging with HaloTag after the C-terminal domain (CTD). (b) Cumulative super-resolution images rendered from single molecule localization from 1000 sequentially recorded frames (96 ms/frame, 96 s in total). (c) Merged triple-color colocalization image of PINK1, Tom20, and respiratory complex I CI. (d) Dual-color SR images. (e) Co-localized molecules determined with open source Fiji ImageJ @ colocalization plugin. (f) Averaged cross line fluorescence distribution profiles of PINK1, Tom20, and CI. The average cross distribution was obtained by averaging up to 30 parallel oriented cross lines (interval 40 nm) per mitochondrion in the framed region of c (see also Supporting Information Figure S3). Scale bar: 1 μm. Images are pseudocolored.

subcompartments. TALM is based on monitoring a limited ensemble of individual target proteins, which are typically integrated or attached to membranes, over time.[26] As these molecules explore their accessible environment by random walk, both the diffusion properties and the dimensions of their microcompartment can be deduced in living cells.[26,27] Recently, we demonstrated that outer and inner mitochondrial membrane proteins could be clearly discriminated by their single molecule localization and trajectory maps.[26] As TALM is based on a relatively small ensemble of labeled molecules, photostable fluorescence dyes are required, which was achieved by post-translational labeling with functionalized tetramethylrhodamine (TMR, emission maximum: 582 nm) via the HaloTag.[28,29] Here, we aimed to achieve dual-color TALM imaging by exploiting a novel silicon-rhodamine (SiR), a red-fluorescent dye (emission maximum: 640 nm) with high photostability recently introduced for high and super-resolution live cell imaging.[30] For orthogonal labeling with TMR and SiR, we combined HaloTag- and $SNAP_f$-tag-specific post-translational conjugation. To this end, we systematically optimized dual-color labeling conditions for single molecule fluorescence microscopy (Supporting Figures S1 and S2). For this purpose, the fusion protein Tom20-$SNAP_f$-HaloTag was generated and double labeled with SiR^{BG} and TMR^{HTL} or TMR-Star and SiR^{HTL}, respectively. We found that labeling of the HaloTag with 1−5 nM TMR^{HTL} or SiR^{HTL} and of the optimized $SNAP_f$ tag[31] with 10−50 nM SiR^{BG} or TMR-Star yielded optimum density of labeled proteins in mitochondrial membranes. The higher concentration of SiR^{BG} is required due to the lower reaction rate constant of $SNAP_f$ substrates with the $SNAP_f$ tag compared to HTL substrates with the HaloTag as quantified by real-time surface-sensitive detection (Supporting Figure S1 and Table S1). The calculated localization precisions of SiR^{BG}, TMR-Star, SiR^{HTL}, and TMR^{HTL} were in the range of 15−33 nm; The signal-to-noise ratios were in the range of 17−27, and the highest emitter intensity was found for TMR-Star (Supporting Figure S2b−d). During time-lapse imaging, a decay of detected molecules was observed with a typical time constant of ∼6 s (200 frames) for both SiR^{BG} and TMR^{HTL}, with 95% bleached molecules after 80 s (Supporting Figure S2e). The delayed bleaching can be explained by partial photoswitching of the dyes, which has been previously reported.[32] These studies established that both dyes could be used for efficient single molecule tracking in living cells.

To pinpoint the localization of PINK1 in mitochondrial subcompartments, we fused the HaloTag to the C-terminus of PINK1 (PINK1-HaloTag), ensuring labeling of both fl-PINK1 and s-PINK1. As reference proteins for localization at the outer mitochondrial membrane (OMM) and the inner mitochondrial membrane (IMM), Tom20 and respiratory complex I (CI), respectively, were used. For this purpose, Tom20 was fused to a C-terminal $SNAP_f$ tag (TOM20-$SNAP_f$) for dual-color TALM while CI was fused to photoactivatable green fluorescent protein (paGFP) for the combination with FPALM to achieve triple-color super-resolution imaging.

We expected that PINK1 and complex I proteins colocalize when the PINK1 kinase domain is imported into mitochondria. To test this, HeLa cells were transiently cotransfected with the three different constructs, and PINK1-HaloTag and TOM20-$SNAP_f$ were labeled with TMR^{HTL} and SiR^{BG}, respectively. To ensure minimal crosstalk between the three channels, sequential excitation of SiR (640 nm), TMR (561 nm), and paGFP (488 nm) was used with a readout time of 32 ms for each channel, yielding a total frame rate of ∼10 Hz. Typically, 1000 frames were recorded (96 s acquisition time), which is owed to the bleaching kinetics of TMR and SiR. This time frame is also tolerable with respect to mitochondrial movement in live cells (own observations). Depending on the respective degree of labeling, after sufficient bleaching, individual molecules could be clearly discerned in all three channels (Video 1, Supporting Figure S2e). The point spread functions of signals derived from single molecules were fitted with a modified 2D Gaussian mask using the Thomson blurring.[33]

DOI: 10.1021/acschembio.5b00295
ACS Chem. Biol. 2015, 10, 1970−1976

The average localization precisions calculated for the three channels were 23 ± 6 nm for paGFP, 26 ± 6 nm for TMR, and 22 ± 7 nm for SiR (Supporting Table S2). SR images were reconstructed by a cumulative overlay of localized molecules from 1000 subsequent frames rendered with the Gaussian profile according to their localization precision (Figure 1b). The overlay of all three channels (Figure 1c) yielded triple-color SR images, revealing distinct localizations of Tom20 (blue), PINK1 (red), and CI (green). The signals of Tom20 show the broadest distribution across single mitochondria. Pairwise colocalization analysis of PINK1 and CI, PINK1 and Tom20, as well as CI and Tom20 from dual-color composite images (Figure 1d) identified the highest overlap of PINK1 and CI signals with a Pearson's coefficient of $P_{\text{PINK1-CI}} = 0.318$. The overlap between PINK1 and Tom20 was noticeably lower ($P_{\text{PINK1-Tom20}} = 0.171$, Figure 1e), while the overlap between CI and Tom20 was negligible ($P_{\text{CI-Tom20}} = 0.035$) in agreement with their strict localization in distinct mitochondrial subcompartments. These observations suggested import of PINK1 across the IMM, which was corroborated by the averaged cross-section fluorescence profiles of PINK1-HaloTag-TMR$^{\text{HTL}}$ and CI-paGFP yielding similar Gaussian-like distribution patterns. In contrast, the cross section profile of Tom20 exhibited two peaks as expected for a protein localized in the OMM (Figure 1f).

To explore the role of the mitochondrial membrane potential in regulating PINK1 processing, we recorded the distribution of PINK1-HaloTag labeled with TMR in depolarized mitochondria, where PINK1 is assumed to initiate mitochondrial clearance at the outside of mitochondria.[20] For depolarization, the protonophore carbonyl cyanide *m*-chlorophenyl hydrazone (CCCP) was added in a concentration (1 μM) sufficient to destroy the membrane potential (data not shown), but too low to immediately induce mitochondrial fragmentation. Triple color SR microscopy performed with CCCP treated cells (Figure 2) revealed a substantially reduced overlay of the PINK1 distribution pattern with CI, while increased overlap with Tom20 was observed (Figure 2a). Also, PINK1 and Tom20 showed a broader distribution than CI (Figure 2b). In the dual-color images, PINK1 and Tom20 showed the highest colocalization ($P = 0.388$), while the distribution profiles of CI and PINK1 ($P = 0.099$) and CI and Tom20 ($P = 0.096$), respectively, were clearly different (Figure 2c). In the cross-section, PINK1-HaloTag-TMR$^{\text{HTL}}$ had no longer a Gaussian distribution profile but displayed two peaks similar to Tom20 (Figure 2d). This is in line with previous biochemical results that PINK1 is found at the OMM in depolarized mitochondria.[20]

The difference in PINK1 distribution between energized and depolarized mitochondria was confirmed by single color SR imaging, where PINK1 showed a clear Gaussian distribution inside energized mitochondria but had a broadened distribution with two peaks in CCCP- and valinomycin-treated mitochondria. Both inhibitors are ionophores that dissipate the membrane potential $\Delta\psi_m$ (Supporting Figure S4). Nigericin, which destroys the ΔpH but not $\Delta\psi_m$, had no effect on import of fl-PINK1. Thus, the retention of PINK1 at the OMM was induced by dissipation of the membrane potential, but not by loss of ΔpH in accordance with previous suggestions.[34] Together, our SR data strongly support the hypothesis that fl-PINK1 is entirely localized inside energized mitochondria but outside of depolarized mitochondria. This would allow for access to different substrates for the kinase in different microcompartments.

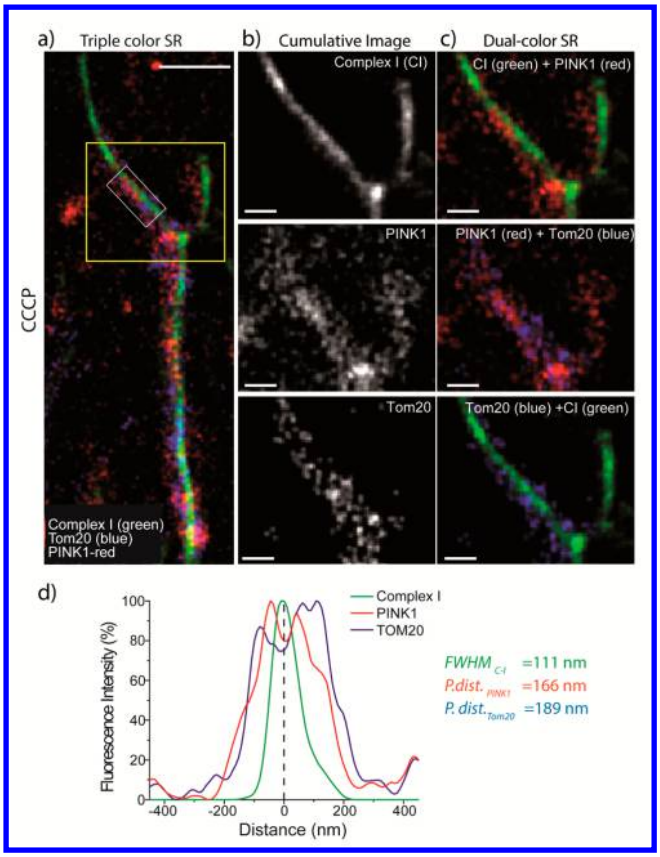

Figure 2. Localization profiles of PINK1, Tom20, and complex I in depolarized mitochondria. Depolarization was achieved by the addition of the protonophore CCCP (1 μM CCCP for 1 h). (a) Triple color super-resolution image rendered from 1000 frames of respiratory complex CI-paGFP, PINK1-HaloTag-TMR$^{\text{HTL}}$ (5 nM TMR$^{\text{HTL}}$), and Tom20-SNAPf-SiR$^{\text{BG}}$ (50 nM SiR$^{\text{BG}}$). The white box indicates the area used to generate the cross-section distribution profile in d. The yellow box indicates the area shown as a detailed close-up of a region of interest (ROI) in images b and c. (b) Cumulative images of single localized emitters (CI; PINK1; Tom20). (c) Cumulative dual-color composite images of CI and PINK1, PINK1 and Tom20, and Tom20 and CI. (d) The average intensity for the cross-section framed in a was determined across the area of the selected region of interest in the mitochondrion as described in the Supporting Information. Scale bars: 1 μm (a), 300 nm (b, c). Images are pseudocolored. FWHM: full width at half-maximum of a Gaussian distribution profile. *P. dist.*: Peak distance.

Importantly, live cell single molecule localization techniques filter for molecules, which do not substantially change their position during the readout time. The ability to localize individual PINK1 at a readout time of 32 ms suggested relatively slow diffusion of PINK1, which was further explored by single molecule tracking (SMT). SMT generates dynamic maps of tracked molecules, providing information about molecular dynamics in cell membranes. (Freely diffusing molecules in aqueous solution are too fast to be tracked due to their at least 100-fold higher diffusion rates). Localized molecules of PINK1 in energized and depolarized mitochondria were connected by a multitarget tracing algorithm[35] when reappearing in subsequent frames (Figure 3a,b). From the tracked molecules, step length histograms were generated and analyzed for mobile, less mobile, and immobile subpopulations

DOI: 10.1021/acschembio.5b00295
ACS Chem. Biol. 2015, 10, 1970−1976

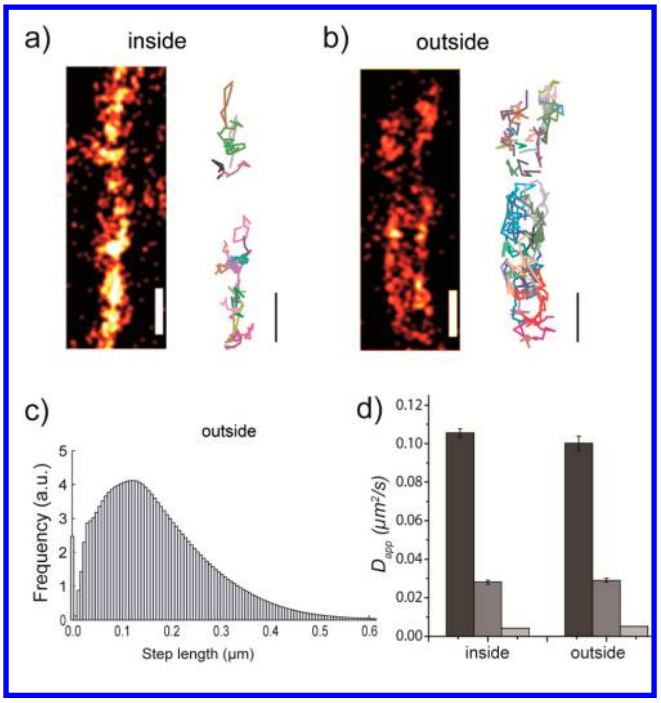

Figure 3. Tracking analysis of PINK1 in the inner and outer membrane of mitochondria. (a) Single color SR image of PINK1 in energized mitochondria with trajectory map. (b) TALM of PINK1 at the outside of de-energized mitochondria. (c) Step-length histogram for PINK1 in CCCP treated mitochondria. Step-length distributions were obtained from single molecule trajectories (5 steps, ~160 ms) and decomposed into diffusive subpopulations by a mixture model of Brownian diffusion. Average diffusion constants D were determined by the slope in mean square displacement analysis (2−10 steps). (d) Apparent diffusion coefficients of PINK1 (D_{app}, $\mu m^2/s$) inside and outside mitochondria. Scale bars: 500 nm (a,b). Images are pseudocolored.

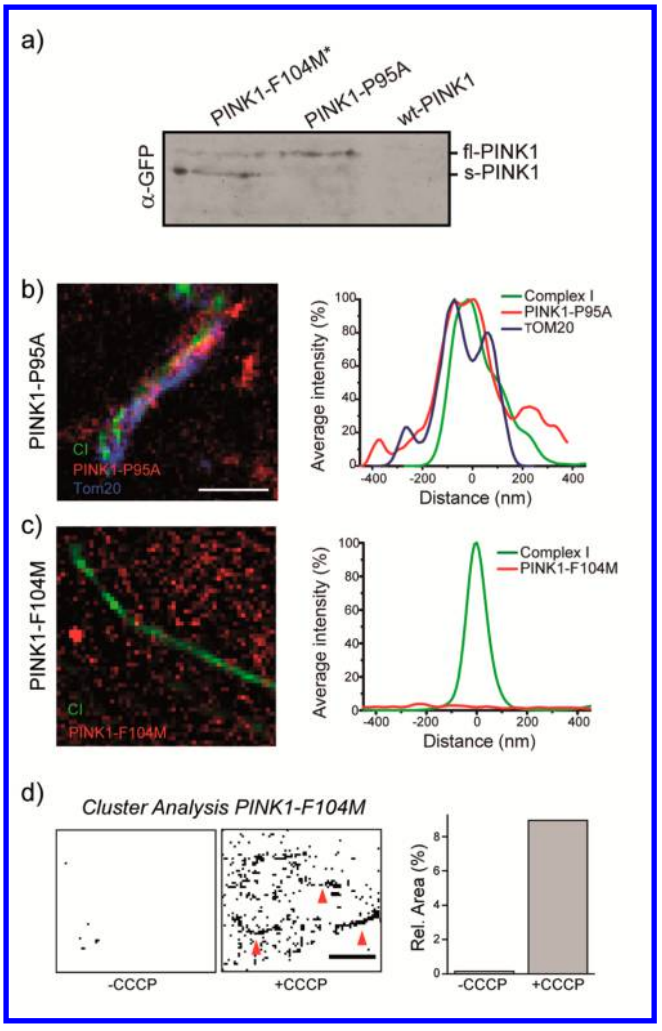

Figure 4. Distribution profiles of PINK1 transmembrane domain mutants. (a) Immuno-blot analysis of PINK1 intermediates in the mutants PINK1-F104A, PINK1-P95A and wt-PINK1. (b) Triple color SR image of PINK1-P95A-HaloTag-SIR^{HTL} (5 nM, red), CI-paGFP (green) and Tom20-$fSNAP_f$-TMR-Star (40 nM, blue) in a single mitochondrion. Right panel: Cross section distribution profiles of PINK1, Tom20 and CI from the same mitochondrion. (c) Dual color SR image of PINK1-F104M-HaloTag-TMR^{HTL} and CI-paGFP. Right panel: Cross section distribution profile of PINK1-F104M and CI-paGFP. (d) Cluster analysis of PINK1 distribution before and after addition of CCCP to cells. Scale bars: 1 μm (b,c), 5 μm (d).

by distribution fits (2−3 fractions), and the respective apparent diffusion coefficients (D_{app}) for two-dimensional diffusion were determined. Molecules with a diffusion coefficient below $D_{app} \leq 0.005\ \mu m^2/s$ were declared immobile. The comparison between PINK1 localized inside and outside mitochondria yielded no significant difference for apparent diffusion coefficients or fractions of mobile/immobile proteins. Mobile PINK1 had an average diffusion coefficient of 0.102 $\mu m^2/s$ (0.004 $\mu m^2/s$ s.d.) inside mitochondria and 0.100 $\mu m^2/s$ (0.004 $\mu m^2/s$ s.d.) outside mitochondria after CCCP treatment. This is 200-times slower than GFP diffusion in the mitochondrial matrix[36] and similar to diffusion of Tom20 (D_{app} = 0.14 ± 0.01 $\mu m^2/s$).[26] From these data, we conclude that PINK1 is either inserted via its TM into the IMM, or associated with integral membrane proteins of the OMM. A likely association of PINK1 with the TOM complex in depolarized mitochondria was reported before.[20]

To validate this interpretation, we explored the localization of the mutants PINK1-F104M and PINK1-P95A, both with mutations in the transmembrane domain in the N-terminal part (cf. Figure 1a). In previous studies, both mutants showed altered processing.[16] We transiently expressed PINK1-F104M-mEGFP and PINK1-P95A-mEGFP in sister cell lines and checked the cleavage of the respective proteins by immuno-blotting against GFP. For the F104M mutation, we confirmed an increase of the PARL-cleaved s-PINK1, while for P95A, reduced PINK1 cleavage was observed (Figure 4a). For wt-PINK1-mEGFP, neither version could be detected due to the high protein turnover associated with low steady state levels of the wt form (Figure 4a).

We then determined the localization of the PINK1 mutants and their processed forms by SR imaging *in situ*. HeLa cells were triple-transfected with PINK1-P95A-HaloTag (stained with SIR^{HTL}), Tom20-$SNAP_f$ (stained with TMR-Star), and CI-paGFP.

The merged image of single localized molecules and the cross section distribution analysis (Figure 4b) revealed an intermediate distribution profile for PINK1-P95A. The profile of the cross-section plot suggests that PINK1-P95A is localized both at the mitochondrial surface and at the IMM. Also, the similar Pearson's coefficients for CI-PINK1 and PINK1-Tom20 confirmed this result (Supporting Figure S5). We explain this distribution by PINK1-P95A being imported into mitochondria but not being efficiently cleaved by PARL.

DOI: 10.1021/acschembio.5b00295
ACS Chem. Biol. 2015, 10, 1970−1976

Because of the impaired processing, also some PINK1 remains at the mitochondrial surface. MTS-fl-PINK1 (OMM) and fl-PINK1 (IMM) cannot be distinguished by SDS PAGE. In contrast to PINK1-P95A, PINK1-F104M was exclusively found in the cytosol as the dual-color SR image clearly shows (Figure 4c). From the size (Figure 4a), we assume that this is the processed s-PINK1 form, which as s-PINK1-F104M is supposed to be more stable than wt-s-PINK1 according to the N-end rule.[21]

We then asked how depolarization of mitochondria (and thus inhibition of fl-PINK1 processing) would influence the spatiotemporal organization of PINK1-F104M. For this purpose, we subjected TALM images of PINK1-F104M to cluster analysis. Owing to the fact that the same set of molecules is detected in each frame in a spatiotemporally correlated manner, such cluster analysis filters for molecules with relatively low mobility as expected for membrane-bound species. Strikingly, we found a significantly increased number of PINK1-F104M clusters in CCCP-treated cells compared to untreated cells (Figure 4d). Some cluster arrangements reproduce the shape of mitochondria (red arrowheads in Figure 4d and Supporting Figure S6). These observations suggest that PINK1-F104M was retained at the OMM of depolarized mitochondria.

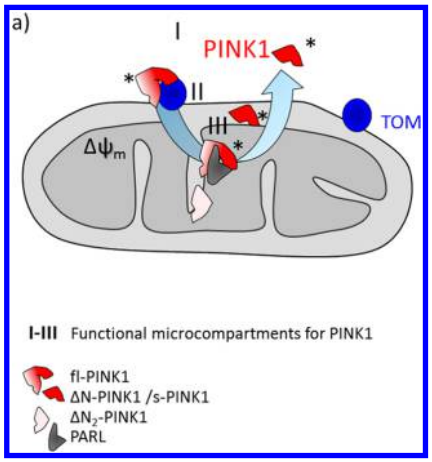

Figure 5. Processing and shuttling of PINK1 through mitochondria is conformed to at least three possible functional microcompartments for PINK1 activity (I, cytosol; II, outer mitochondrial membrane; III, inside mitochondria) allowing for interaction with different substrates (*).

In conclusion, we here have established dual-color TALM imaging in combination with FPALM as a powerful approach for unraveling the spatiotemporal organization of suborganelle microcompartments, which have important implications for many cellular functions.[37] In contrast to previously established live-cell triple-color SR imaging based on FPALM and dSTORM,[38,39] TALM-based imaging in addition provides detailed information on protein dynamics within micro-compartments as individual molecules are tracked for comparably long time periods.[26] Tackling the intricate problem of intramitochondrial trafficking of PINK1, we exploited this specific feature of TALM to not only resolve protein distribution beyond the diffraction limit but also to provide detailed information on diffusion dynamics and diffusional connectivity. Our data support the following model of PINK1 shuttling: (i) import of the complete fl-PINK1 protein including the kinase domain into mitochondria tightly coupled to (ii) proteolytic processing (probably by PARL) in the inner mitochondrial membrane in a $\Delta\Psi_m$-dependent manner; (iii) export of the short form with the kinase domain into the cytosol (Figure 5). This process in principle provides at least three possible sites for PINK1 activity: at the IMM inside mitochondria, at the OMM, and in the cytosol. Diffusional data moreover suggest that PINK1 remains membrane-associated during trafficking in mitochondria.

Overall, these results highlight some key advantages of TALM imaging for the spatiotemporal analysis of protein distribution, in particular for studying proteins with high turnover and low steady state concentration of intermediates.

■ ASSOCIATED CONTENT

Supporting Information

Experimental procedures, imaging conditions, and supporting figures are included. The Supporting Information is available free of charge on the ACS Publications website at DOI: 10.1021/acschembio.5b00295.

■ AUTHOR INFORMATION

Corresponding Author

*E-mail: buschkar@uni-muenster.de.

Present Addresses

[†]Institute of Complex Systems 4 (ICS-4), Cellular Biophysics, Forschungszentrum Jülich GmbH, 52425 Jülich, Germany

[‡]Institute of Molecular Cell Biology and Mitochondrial Dynamics, University of Münster, 48149 Münster, North Rhine-Westphalia, Germany

Notes

The authors declare no competing financial interest.

■ ACKNOWLEDGMENTS

The SIR-^{BG} was a kind gift of K. Johnsson. We thank Christian Richter for the development of image analysis software, Rainer Kurre for technical support with the microscopic set-up and Wladislaw Kohl for technical assistance. This work was supported by the German National Research Foundation grant Bu2288/1-2 and the SFB944.

■ ABBREVIATIONS

CI, complex I; CCCP, carbonyl cyanid-*m*-chlorophenyl hydrazine; FPALM, fluorescence photoactivation localization microscopy; HTL, HaloTag ligand; IMM, inner mitochondrial membrane; IMS, intermembrane space; MTS, mitochondrial targeting sequence; OMM, outer mitochondrial membrane; TALM, tracking and localization microscopy; TM, transmembrane domain; TMR, tetramethylrhodamine; SiR, siliconrhodamine; SR, super-resolution; dSTORM, stochastic optical reconstruction microscopy

■ REFERENCES

(1) Narendra, D. P., and Youle, R. J. (2011) Targeting mitochondrial dysfunction: role for PINK1 and Parkin in mitochondrial quality control. *Antioxid. Redox Signaling 14*, 1929−1938.

(2) Jin, S. M., and Youle, R. J. (2012) PINK1- and Parkin-mediated mitophagy at a glance. *J. Cell Sci. 125*, 795−799.

(3) McLelland, G.-L., Soubannier, V., Chen, C. X., McBride, H. M., and Fon, E. A. (2014) Parkin and PINK1 function in a vesicular trafficking pathway regulating mitochondrial quality control. *EMBO J. 33*, 282−295.

DOI: 10.1021/acschembio.5b00295
ACS Chem. Biol. 2015, 10, 1970−1976

(4) Vincow, E. S., Merrihew, G., Thomas, R. E., Shulman, N. J., Beyer, R. P., MacCoss, M. J., and Pallanck, L. J. (2013) The PINK1−Parkin pathway promotes both mitophagy and selective respiratory chain turnover in vivo. *Proc. Natl. Acad. Sci. U. S. A. 110*, 6400−6405.
(5) Murata, H., Sakaguchi, M., Jin, Y., Sakaguchi, Y., Futami, J.-i., Yamada, H., Kataoka, K., and Huh, N.-h. (2011) A new cytosolic pathway from a Parkinson disease-associated kinase, BRPK/PINK1: activation of AKT via mTORC2. *J. Biol. Chem. 286*, 7182−7189.
(6) Weihofen, A., Thomas, K. J., Ostaszewski, B. L., Cookson, M. R., and Selkoe, D. J. (2009) Pink1 Forms a Multiprotein Complex with Miro and Milton, Linking Pink1 Function to Mitochondrial Trafficking RID A-1566-2011. *Biochemistry 48*, 2045−2052.
(7) Kondapalli, C., Kazlauskaite, A., Zhang, N., Woodroof, H. I., Campbell, D. G., Gourlay, R., Burchell, L., Walden, H., Macartney, T. J., Deak, M., Knebel, A., Alessi, D. R., and Muqit, M. M. (2012) PINK1 is activated by mitochondrial membrane potential depolarization and stimulates Parkin E3 ligase activity by phosphorylating Serine 65. *Open Biol. 2*, 120080.
(8) Pridgeon, J. W., Olzmann, J. A., Chin, L.-S., and Li, L. (2007) PINK1 protects against oxidative stress by phosphorylating mitochondrial chaperone TRAP1. *PLoS Biol. 5*, 1494−1503.
(9) Plun-Favreau, H., Klupsch, K., Moisoi, N., Gandhi, S., Kjaer, S., Frith, D., Harvey, K., Deas, E., Harvey, R. J., McDonald, N., Wood, N. W., Martins, L. M., and Downward, J. (2007) The mitochondrial protease HtrA2 is regulated by Parkinson's disease-associated kinase PINK1 RID C-8513−2009 RID A-6755−2010 RID C-2505−2009. *Nature Cell Biol. 9*, 1243−U1263.
(10) Morais, V. A., Haddad, D., Craessaerts, K., De Bock, P.-J., Swerts, J., Vilain, S., Aerts, L., Overbergh, L., Grünewald, A., Seibler, P., Klein, C., Gevaert, K., Verstreken, P., and De Strooper, B. (2014) PINK1 Loss of Function Mutations Affect Mitochondrial Complex I Activity via NdufA10 Ubiquinone Uncoupling. *Science (New York, N.Y.) 344*, 203.
(11) Tatsuta, T., and Langer, T. (2008) Quality control of mitochondria: protection against neurodegeneration and ageing. *EMBO J. 27*, 306−314.
(12) Twig, G., Elorza, A., Molina, A. J., Mohamed, H., Wikstrom, J. D., Walzer, G., Stiles, L., Haigh, S. E., Katz, S., Las, G., Alroy, J., Wu, M., Py, B. F., Yuan, J., Deeney, J. T., Corkey, B. E., and Shirihai, O. S. (2008) Fission and selective fusion govern mitochondrial segregation and elimination by autophagy. *EMBO J. 27*, 433−446.
(13) Greene, A. W., Grenier, K., Aguileta, M. A., Muise, S., Farazifard, R., Haque, M. E., McBride, H. M., Park, D. S., and Fon, E. A. (2012) Mitochondrial processing peptidase regulates PINK1 processing, import and Parkin recruitment. *EMBO Rep. 13*, 378−385.
(14) Meissner, C., Lorenz, H., Weihofen, A., Selkoe, D. J., and Lemberg, M. K. (2011) The mitochondrial intramembrane protease PARL cleaves human Pink1 to regulate Pink1 trafficking. *J. Neurochem. 117*, 856−867.
(15) Whitworth, A. J., Lee, J. R., Ho, V. M., Flick, R., Chowdhury, R., and McQuibban, G. A. (2008) Rhomboid-7 and HtrA2/Omi act in a common pathway with the Parkinson's disease factors Pink1 and Parkin. *Dis. Models Mech. 1*, 168−174 discussion 173..
(16) Deas, E., Plun-Favreau, H., Gandhi, S., Desmond, H., Kjaer, S., Loh, S. H., Renton, A. E., Harvey, R. J., Whitworth, A. J., Martins, L. M., Abramov, A. Y., and Wood, N. W. (2011) PINK1 cleavage at position A103 by the mitochondrial protease PARL. *Hum. Mol. Genet. 20*, 867−879.
(17) Jin, S. M., Lazarou, M., Wang, C., Kane, L. A., Narendra, D. P., and Youle, R. J. (2010) Mitochondrial membrane potential regulates PINK1 import and proteolytic destabilization by PARL. *J. Cell Biol. 191*, 933−942.
(18) Lin, W., and Kang, U. J. (2008) Characterization of PINK1 processing, stability, and subcellular localization. *J. Neurochem. 106*, 464−474.
(19) Becker, D., Richter, J., Tocilescu, M. A., Przedborski, S., and Voos, W. (2012) Pink1 and its {Delta}ψ-dependent cleavage product both localize to the outer mitochondrial membrane by a unique targeting mode. *J. Biol. Chem. 287*, 22969.
(20) Lazarou, M., Jin, S. M., Kane, L. A., and Youle, R. J. (2012) Role of PINK1 binding to the TOM complex and alternate intracellular membranes in recruitment and activation of the E3 ligase Parkin. *Dev. Cell 22*, 320−333.
(21) Yamano, K., and Youle, R. J. (2013) PINK1 is degraded through the N-end rule pathway. *Autophagy 9*, 1758−1769.
(22) Zhou, C., Huang, Y., Shao, Y., May, J., Prou, D., Perier, C., Dauer, W., Schon, E. A., and Przedborski, S. (2008) The kinase domain of mitochondrial PINK1 faces the cytoplasm. *Proc. Natl. Acad. Sci. U.S.A. 105*, 12022−12027.
(23) Silvestri, L., Caputo, V., Bellacchio, E., Atorino, L., Dallapiccola, B., Valente, E., and Casari, G. (2005) Mitochondrial import and enzymatic activity of PINK1 mutants associated to recessive parkinsonism. *Hum. Mol. Genet. 14*, 3477−3492.
(24) Betzig, E., Patterson, G. H., Sougrat, R., Lindwasser, O. W., Olenych, S., Bonifacino, J. S., Davidson, M. W., Lippincott-Schwartz, J., and Hess, H. F. (2006) Imaging Intracellular Fluorescent Proteins at Nanometer Resolution. *Science 313*, 1642−1645.
(25) Hess, S. T., Girirajan, T. P. K., and Mason, M. D. (2006) Ultra-High Resolution Imaging by Fluorescence Photoactivation Localization Microscopy. *Biophys. J. 91*, 4258−4272.
(26) Appelhans, T., Richter, C. P., Wilkens, V., Hess, S. T., Piehler, J., and Busch, K. B. (2012) Nanoscale organization of mitochondrial microcompartments revealed by combining tracking and localization microscopy. *Nano Lett. 12*, 610−616.
(27) You, C., Richter, C. P., Lochte, S., Wilmes, S., and Piehler, J. (2014) Dynamic submicroscopic signaling zones revealed by pair correlation tracking and localization microscopy. *Anal. Chem. 86*, 8593−8602.
(28) Stagge, F., Mitronova, G. Y., Belov, V. N., Wurm, C. A., and Jakobs, S. (2013) Snap-, CLIP- and Halo-Tag Labelling of Budding Yeast Cells. *PLoS One 8*, e78745.
(29) Los, G. V., Encell, L. P., McDougall, M. G., Hartzell, D. D., Karassina, N., Zimprich, C., Wood, M. G., Learish, R., Ohana, R. F., Urh, M., Simpson, D., Mendez, J., Zimmerman, K., Otto, P., Vidugiris, G., Zhu, J., Darzins, A., Klaubert, D. H., Bulleit, R. F., and Wood, K. V. (2008) HaloTag: a novel protein labeling technology for cell imaging and protein analysis. *ACS Chem. Biol. 3*, 373−382.
(30) Lukinavicius, G., Umezawa, K., Olivier, N., Honigmann, A., Yang, G., Plass, T., Mueller, V., Reymond, L., Correa, I. R., Jr., Luo, Z. G., Schultz, C., Lemke, E. A., Heppenstall, P., Eggeling, C., Manley, S., and Johnsson, K. (2013) A near-infrared fluorophore for live-cell super-resolution microscopy of cellular proteins. *Nat. Chem. 5*, 132−139.
(31) Juillerat, A., Gronemeyer, T., Keppler, A., Gendreizig, S., Pick, H., Vogel, H., and Johnsson, K. (2003) Directed evolution of O6-alkylguanine-DNA alkyltransferase for efficient labeling of fusion proteins with small molecules in vivo. *Chem. Biol. 10*, 313−317.
(32) Heilemann, M., van de Linde, S., Schuttpelz, M., Kasper, R., Seefeldt, B., Mukherjee, A., Tinnefeld, P., and Sauer, M. (2008) Subdiffraction-resolution fluorescence imaging with conventional fluorescent probes. *Angew. Chem., Int. Ed. Engl. 47*, 6172−6176.
(33) Thompson, R. E., Larson, D. R., and Webb, W. W. (2002) Precise nanometer localization analysis for individual fluorescent probes. *Biophys. J. 82*, 2775−2783.
(34) Narendra, D., Tanaka, A., Suen, D. F., and Youle, R. J. (2009) Parkin-induced mitophagy in the pathogenesis of Parkinson disease. *Autophagy 5*, 706−708.
(35) Sergé, A., Bertaux, N., Rigneault, H., and Marguet, D. (2008) Dynamic multiple-target tracing to probe spatiotemporal cartography of cell membranes. *Nat. Methods 5*, 687−694.
(36) Verkman, A. S. (2002) Solute and macromolecule diffusion in cellular aqueous compartments. *Trends Biochem. Sci. 27*, 27−33.
(37) Holthuis, J. C., and Ungermann, C. (2013) Cellular microcompartments constitute general suborganellar functional units in cells. *Biol. Chem. 394*, 151−161.
(38) Gunewardene, M. S., Subach, F. V., Gould, T. J., Penoncello, G. P., Gudheti, M. V., Verkhusha, V. V., and Hess, S. T. (2011) Superresolution imaging of multiple fluorescent proteins with highly

DOI: 10.1021/acschembio.5b00295
ACS Chem. Biol. 2015, 10, 1970−1976

overlapping emission spectra in living cells. *Biophys. J. 101*, 1522−1528.
(39) Wilmes, S., Staufenbiel, M., Lisse, D., Richter, C. P., Beutel, O., Busch, K. B., Hess, S. T., and Piehler, J. (2012) Triple-color super-resolution imaging of live cells: resolving submicroscopic receptor organization in the plasma membrane. *Angew. Chem., Int. Ed. Engl. 51*, 4868−4871.

DOI: 10.1021/acschembio.5b00295
ACS Chem. Biol. 2015, 10, 1970−1976